Abstract

STUDY DESIGN: An association study investigating the genetic etiology for spinal osteoarthritis.

OBJECTIVE: To determine the association of single-nucleotide polymorphism (SNP) causing an amino-acid change (Q89R) in the low-density lipoprotein receptor-related protein 5 (LRP5) coding region with spinal osteoarthritis.

SUMMARY OF BACKGROUND DATA: Wnt/β-catenin signaling pathway regulates bone density through a Wnt co-receptor LRP5. This pathway is also involved in cartilage development and homeostasis, suggesting that genetic variation in LRP5 gene may affect the pathogenesis of cartilage-related diseases, such as osteoarthritis.

METHODS: We evaluated the presence of osteophytes, endplate sclerosis, and narrowing of disc spaces in 357 Japanese postmenopausal women. Missense coding SNP for Q89R of LRP5 gene was determined using TaqMan polymerase chain reaction (PCR) method.

RESULTS: We found that subjects without the R allele (QQ; n = 321) had a significantly lower osteophyte formation score than did subjects bearing at least one R allele (QR + RR; n = 36) (7.80 *vs.* 10.89, $P = 0.0019$ by analysis of covariance).

CONCLUSIONS: We suggest that a genetic variation at the LRP5 gene locus is associated with spinal osteoarthritis, in line with the involvement of the LRP5 gene in the bone and cartilage metabolism.

Key Words

Single-nucleotide polymorphism (SNP), Low-density lipoprotein receptor-related protein 5 (LRP5), spinal osteoarthritis, osteophytosis

Key Points

Wnt/β-catenin signaling pathway regulates bone and cartilage metabolism. The single-nucleotide polymorphism causing an amino-acid change (Q89R) in LRP5 gene that encodes a Wnt co-receptor, was associated with spinal osteophytosis in Japanese postmenopausal women. We suggest that a genetic variation at the LRP5 gene locus is associated with spinal osteoarthritis.

Mini Abstract

Wnt/β-catenin signaling pathway regulates bone and cartilage metabolism. The single nucleotide polymorphism causing an amino-acid change (Q89R) in LRP5 gene, a Wnt co-receptor, was associated with spinal osteophytosis in Japanese postmenopausal women. We suggest that a genetic variation at the LRP5 gene locus is associated with spinal osteoarthritis.

Introduction

Osteoarthritis of the spine is a very common condition in the axial skeletons of aged people [1]. Vertebral osteophytes, endplate sclerosis and intervertebral disc narrowing are recognized as characteristic features of spinal degeneration. Recent studies indicate that the appearance of these radiographical features is influenced by genetic factors, physical loading and other environmental factors [2,3]. Association studies in using various definitions of osteoarthritis have been performed, mainly investigating genes encoding structural proteins of the extracellular matrix of cartilage (e.g. collagen type II α1, cartilage matrix protein, and aminoguanidine) or genes playing a role in the regulation of bone density and mass (e.g. vitamin D receptor, insulin-like growth factor-I, and estrogen receptor α) [4,5].

The Wnt (wingless-type MMTV integration site family) represents a large group of secreted signaling proteins that are involved in cell proliferation, differentiation and morphogenesis [6]. The name of 'Wnt' is derived from *wingless* gene in Drosophila melanogaster [7] and murine *int-1* oncogene identified in tumors induced by mouse mammary tumor virus [8]. It is also known that Wnt and bone morphogenetic protein (BMP) signals control apical ectodermal ridge (AER) formation and dorsal-ventral patterning during limb development [9,10]. Wnt proteins activate signal transduction through Frizzled which act as receptors for Wnt proteins [11] and induce stabilization of cytoplasmic β-catenin protein, which also regulates target gene expression as a transcriptional co-activator. The physiological role of Wnt in the regulation of osteoblastogenesis has been studied in experimental models, in embryonic mesenchymal progenitor cells expressing Wnt3a [12] or in mice expressing Wnt10b transgene in bone marrow [13]. It is also shown that activated β-catenin modulate osteoblast and chondrocyte differentiation [14,15]. Meanwhile, LDL receptor-related protein 5 and 6 (LRP5/6) were also found to be required for Wnt co-receptors [16,17]. Recent reports demonstrated that the Wnt/β-catenin signaling pathway regulates bone density of whole body through LRP5 [18-21]. These findings indicate that Wnt-β-catenin signaling pathway plays important roles in the skeletal biology.

In addition to the regulation of limb development and bone metabolism, Wnt/β-catenin signaling may be involved in maintenance and pathophysiology of cartilage. This possibility is indirectly supported by the observation that several Wnt proteins and Frizzled receptors are expressed in synovial tissue of arthritic cartilage [22]. In addition, a secreted Frizzled-related protein (FrzB-2) that act as an antagonist for Frizzled receptor is strongly expressed in osteoarthritic cartilage and may regulate chondrocyte apoptosis [23]. It is also reported that chondrocytes express β-catenin at a low level and accumulation of β-catenin is sufficient to cause dedifferentiation of chondrocytes, suggesting that Wnt signaling is involved in cartilage metabolism [24]. Thus, it is assumed that LRP5 modulates Wnt/β-catenin signaling pathway in the bone and cartilage homeostasis. In the present study, we examine an association between a polymorphism in LRP5 gene and radiographic feautures of spinal osteoarthritis including osteophyte formation, endplate sclerosis and disc space narrowing number to investigate a possible contribution of LRP5 to human bone and cartilage metabolism.

Materials and methods

Subjects

Genotypes were analyzed in DNA sample obtained from 357 healthy postmenopausal Japanese women (mean age + SD; 65.22 + 8.20) living in central area of Japan. Exclusion criteria included endocrine disorders such as hyperthyroidism, hyperparathyroidism, diabetes mellitus, liver disease, renal disease, use of medications known to affect bone metabolism (e.g. corticosteroids, anticonvulsants, heparin sodium), or unusual gynecologic history. Patients with severe hip and knee arthritis were excluded from the present study. The eligibility of subjects was determined by taking history-physical examination. All were non-related volunteers and provided informed consent before this study. Ethical approval for the study was obtained from appropriate ethics committees.

Radiographic grading of osteoarthritis of the spine

Conventional thoracic and lumbar spinal plain roentgenograms in lateral and anteroposterior projection were obtained from all participants. The severities of spinal degeneration including osteophyte formation, endplate sclerosis and disc space narrowing were assessed semi-quantitatively from Th4/5 to L4/5 disc level or from Th4 to L5 vertebrae by using the grading scale of Genant [25]. Briefly osteophyte formation at a given disc was graded 0-3 degrees, endplate sclerosis at given vertebra was graded 0-2 degrees, and disc space narrowing was graded 0-1 degrees. Then we defined sum of each degree from Th4/5 to L4/5 disc level for osteophyte formation on anteroposterior radiographs as a score of osteophyte formation. We also defined sum of each degree from Th4 to L4 vertebra for endplate sclerosis and that from Th4/5 to L4/5 disc level for disc space narrowing on lateral radiographs as a score of endplate sclerosis and disc narrowing, respectively. Then we defined sum of each thirteen grade for osteophyte formation on anteroposterior radiographs as a score of osteophyte formation. We also defined sum of thirteen grade for endplate sclerosis and disc space narrowing on lateral radiographs as a score of endplate sclerosis and disc narrowing, respectively.

Measurement of bone mineral density (BMD) and biochemical markers

The lumbar-spine BMD and total body BMD (in g/cm^2) of each participant were measured by dual-energy X-ray absorptiometry using fast-scan mode (DPX-L; Lunar, Madison, WI). The BMD data were recorded as 'Z scores'; that is, deviation from the weight-adjusted average BMD for each age. Z scores were calculated using installed software (Lunar DPX-L) on the basis of data from 20,000 Japanese women.

We measured serum concentration of calcium (Ca), phosphate (P), alkaline phosphatase (ALP), intact-osteocalcin (I-OC, ELISA; Teijin, Tokyo, Japan), intact parathyroid hormone (PTH), calcitonin (CT) and 1, 25(OH)2D3. We also measured urinary ratios of urinary deoxypyridinoline (DPD, HPLC method) to creatinine.

Determination of a single nucleotide polymorphism in the LRP5 gene

DNA was extracted from peripheral leukocytes by standard techniques. Missense coding SNP for Q89R (c. 266A>G) of the LRP5 gene was determined using Assays by Design SNP Genotyping Products (Applied BioSystems) that based on the TaqMan PCR method [26]. Missense coding means that the alteration of a codon (an

array of three consecutive bases in mRNA) that encodes a different amino acid. TaqMan PCR method utilizes two kinds of TaqMan probes that correspond to a DNA fragment including the target SNP site with different alleles and the 5'-3' nuclease activity of Taq polymerase that is essential for PCR. TaqMan probes include fluorescence dyes at their 5' ends and a quencher at their 3' ends. During PCR cycles, TaqMan probes will anneal to target DNA and will be excised by the 5'-3' nuclease activity of Taq polymerase if there is no mismatch between the probes and target sequences. Then the fluorescence dyes will be released from the probes and the intensity of fluorescence can be monitered by using ABI PRISM 7000 (Applied Biosystems) as a fluorescence detector. The allele frequencies of Q89R polymorphism were confirmed as they were not significantly deviated from Hardy-Weinberg equilibrium. Since Hardy-Weinberg equilibrium is based on the following assumptions including no genetic drift, no gene flow, no natural selection, negligible mutations, and random mating, the population under the equilibrium is not evolving and its genotype and allele frequencies are predicted to remain unchanged over successive generations. Thus, we considered that our subjects were eligible for the correlation study.

Statistical analysis

We divided subjects into those having one or two chromosomes of the minor G-allele (QR+RR) and those with only the major A-allele (QQ) encoded at the same locus. Comparisons of Z scores of lumbar spine and biochemical markers between these two groups were subjected to statistical analysis (unpaired t-test; StatView-J 4.5, SAS Institute Inc.). The association between these two groups and osteoarthritis parameters (number of osteophyte, endoplate sclerosis and disc narrowing), was assessed by unpaired t-test and by analysis of covariance (ANCOVA) with adjustment of confounding clinical variables (age, body weight, and height). A *P*-value less than 0.05 was considered statistically significant.

Results

We analyzed the genotypes for the SNP of LRP5 at Q89R (c.266 A>G) in subjects, using TaqMan methods. Among 357 postmenopausal Japanese women, 321 were QQ homozygotes, 35 were QR heterozygotes, and 1 were RR homozygotes. The allelic frequencies of this SNP in the present study were in Hardy-Weinberg equilibrium.

Because only one of these subjects carried the RR genotype of the Q89R polymorphism, we compared those who carried the R allele (QR or RR) with those who did not (QQ). The lumbar BMD was not statistically different between these groups (Table 1). The background and biochemical data were not statistically different between these groups (Table 1). On ANCOVA analysis, we found significant associations between LRP5 Q89R genotype and osteophyte formation score after controlling for age, weight and height. Women without the R allele (QQ; n = 321) had a significantly lower osteophyte formation score than did subjects bearing at least one R allele (QR + RR; n = 36) (7.80 ± 6.51 vs 10.89 ± 7.6, $P = 0.0019$, Fig 1A, Table 2). We also found significant

association between them on unpaired t-test (P=0.0083, Table1). On the other hand, the occurrence of disc narrowing and endplate sclerosis did not significantly differ in those with and without at least one R allele (Fig 1B and C, Table 2).

Discussion

The present study is the first report that shows the influence of a single-nucleotide polymorphism of LRP5 gene on spinal osteoarthritis as far as we know. Targeting the pathogenesis of low back pain, we have previously investigated associations of genetic factors with osteoporosis. LRP5 has been shown as one of the correlated genes in Japanese postmenopausal women [27]. Because spinal osteoarthritis is another major reason for low back pain, we have extended our association study of LRP5 polymorphism with spinal osteoarthritis. We demonstrated that the Japanese postmenopausal women who had one or two allele(s) of a non-synonymous change (Q89R) in LRP5 gene showed significantly higher osteophyte formation score of spine. Our finding may also be supported by genome-wide scan for osteoarthritis-susceptibility loci that showed a linkage to chromosome 11q12-13 [28,29], which includes the LRP5 gene locus on 11q13.4. It has been recently shown that single-nucleotide polymorphisms in LRP5 gene provided no correlation with knee osteoarthritis status while haplotype analysis revealed that there was a common haplotype that provided a 1.6-fold increased risk [30], suggesting that LRP5 might be involved in the pathogenesis of osteoarthritis also in other joints. It is also reported that there was a significant association of a functional gene variant of secreted frizzled-related protein 3 (sFRP3), which antagonizes Wnt signaling, with hip osteoarthritis in women [31]. Taken together, our results and the recent evidence suggest that the canonical Wnt signaling pathway including LRP5 is critical in the pathogenesis of skeletal abnormality including osteoarthritis and osteoporosis.

Recently, mutations of the LRP5 gene have been described to be associated with both osteoporosis-pseudoglioma syndrome and the high bone mass phenotype[18-21]. It was found that loss-of-function of LRP5 in both human [18] and mice [19] yielded a decrease in bone formation, or an active mutation of LRP5 that cannot bind to a Wnt inhibitor Dickkopf-1 resulted in a high bone mass trait [20,21]. Moreover, our group and several other groups have reported that single-nucleotide polymorphisms in LRP5 gene predicted the bone mass [27, 32-36]. These SNPs included three of different missense variations; Q89R [33,34], V667M [35], and A1330V [36]. In the present study, we investigated a possible contribution of Q89R LRP5 polymorphism to spinal osteoarthritis in Japanese women. V667M polymorphism was not detected in our Japanese population. Regarding A1330V polymorphism, we could not detect an association of the SNP with spinal osteoarthritis (data not shown).

Two groups reported consistent association of Q89R with Ward's triangle BMD but not with lumbar BMD in Korean young men [33] and Chinese premenopausal women [34]. In our Japanese population, we did not find an association of Q89R polymorphism with lumbar spine. The present data together with published data related

to osteoporosis suggest that Q89R polymorphism may be involved in the pathogenesis of both osteoporosis and spinal osteoarthritis and QQ genotype in LRP5 might be preventive for both diseases. Meanwhile, there are other cases in which genetic factors contribute to the pathogenesis of osteoporosis and osteoarthritis in an opposite way. For example, it has been reported that transforming growth factorβ1 (TGFβ1) gene polymorphism T869C which gives Leu>Pro substitution contributes differentially to osteoporosis and osteoarthritis; people with CC genotype had significantly higher BMD than those with TC or TT, whereas this CC genotype was related to significantly greater osteophytes than TT or TC [37].

Osteoarthritis occurs as result of both mechanical and biological events that destabilize the normal coupling of degradation and synthesis of articular cartilage chondrocytes and extracellular matrix as well as subchondral bone [1,38]. Cartilage destruction during osteoarthritis involves the loss of differentiated phenotype and apoptotic death of chondrocytes [39], Wnt proteins were shown to regulate dedifferentiation of apoptosis of chondrocytes [40]. It is also demonstrated the interaction of β-catenin with SOX9, a transcriptional factor that is required in successive steps of chondrogenesis, control chondrocyte differentiation [41]. These data suggest Wnt/β-catenin may be participated in the pathogenesis of cartilage diseases, such as osteoarthritis. Further studies will be required to clarify the role of Q89R misssense variant of the LRP5 in the pathogenesis of osteophyte formation and osteoporosis.

In conclusion, we have shown an association of the Q89R polymorphism in the LRP5 gene with a radiographic feauture of spinal osteophytosis in postmenopausal Japanese women. The women with QQ genotypes had significantly lower osteophyte formation scores. The LRP5 genotyping might be benefical in the prevention and management of spinal osteophytosis as well as osteoporosis. The present findings regarding the correlation of LRP5 polymorphism with spinal osteoarthritis provide a new promising direction for the clinical medicine of the spine disease, which leads us to the development of new diagnostic markers as well as therapeutic options based on the molecular target.

References

1. Creamer P, Hochberg MC. Osteoarthritis. *Lancet* 1997;350:503-8.
2. Lane NE, Nevitt MC, Hochberg MC, et al. Reliability of new indices of radiographic osteoarthritis of the hand and hip and lumbar disc degeneration. *J Rheumatol* 1993;20:1911-18.
3. O'Neill TW, McCloskey EV, Silman AJ, et al. The distribution, determinants, and clinical correlates of vertebral osteophytosis: a population based survey. *J Rheumatol* 1999;26:842-8.
4. Spector TD, MacGregor AJ. Risk factors for osteoarthritis: genetics. *Osteoarthritis Cartilage* 2004;12:S39-44.
5. Loughlin J. Genetics of osteoarthritis and potential for drug development. *Curr Opin Pharmacol* 2003;3:295-9.

6. Nusse R, Varmus HE. Wnt genes. *Cell* 1992;69:1073-87.
7. Rijsewijk F, Schuermann M, Wagenaar E, et al. The Drosophila homolog of the mouse mammary oncogene int-1 is identical to the segment polarity gene wingless. *Cell* 1987;50:649-57.
8. Nusse R, Varmus HE. Many tumors induced by the mouse mammary tumor virus contain a provirus integrated in the same region of the host genome. *Cell* 1982;31:99-109.
9. Barrow JR, Thomas KR, Boussadia-Zahui O, et al. Ectodermal Wnt3/beta-catenin signaling is required for the establishment and maintenance of the apical ectodermal ridge. *Genes Dev* 2003;17:394-409.
10. Soshnikova N, Zechner D, Huelsken J, et al. Genetic interaction between Wnt/beta-catenin and BMP receptor signaling during formation of the AER and the dorsal-ventral axis in the limb. *Genes Dev* 2003;17:1963-8.
11. Cadigan KM, Nusse R. Wnt signaling: a common theme in animal development. *Genes Dev* 1999;11:3286-305.
12. Derfoul A, Carlberg AL, Tuan RS, et al. Differential regulation of osteogenic marker gene expression by Wnt-3a in embryonic mesenchymal multipotential progenitor cells. *Differentiation* 2004;72:209-23.
13. Bennett CN, Longo KA, Wright WS, et al. Regulation of osteoblastogenesis and bone mass by Wnt10b. *Proc Natl Acad Sci U S A* 2005;102:3324-9.
14. Bain G, Muller T, Papkoff J, et al. Activated beta-catenin induces osteoblast differentiation of C3H10T1/2 cells and participates in BMP2 mediated signal transduction. *Biochem Biophys Res Commun* 2003;301:84-91.
15. Zhou S, Eid K, Glowacki J. Cooperation between TFG-beta and Wnt pathways during chondrocyte and adipocyte differentiation of human marrow stromal cells. *J Bone Miner Res* 2004;19:463-70.
16. Tamai K, Semenov M, Kato Y, et al. LDL-receptor-related proteins in Wnt signal transduction. *Nature* 2000;407:530-5.
17. Mao J, Wang J, Liu B, et al. Low-density lipoprotein receptor-related protein-5 binds to Axin and regulates the canonical Wnt signaling pathway. *Mol Cell* 2001;7:801-9.
18. Gong Y, Slee RB, Fukai N, et al. LDL receptor-related protein 5 (LRP5) affects bone accrual and eye development. *Cell* 2001;107:513-23.
19. Kato M, Patel MS, Levasseur R, et al. Cbfa1-independent decrease in osteoblast proliferation, osteopenia, and persistent embryonic eye vascularization in mice deficient in Lrp5, a Wnt coreceptor. *J Cell Biol* 2002;157:303-14.
20. Boyden LM, Mao J, Belsky J, et al. High bone density due to a mutation in LDL-receptor-related protein 5. *N Engl J Med* 2002;346:1513-21.
21. Little RD, Carulli JP, Del Mastro RG, et al. A mutation in the LDL receptor-related protein 5 gene results in the autosomal dominant high-bone-mass trait. *Am J Hum Genet* 2002;70:11-9.
22. Sen M, Lauterbach K, Carson DA, et al. Expression and function of wingless and frizzled homologs in rheumatoid arthritis. *Proc Natl Acad Sci USA* 2000;97:2791-6.
23. James IE, Kumar S, Lark MW, et al. FrzB-2: a human secreted frizzled-related protein with a potential role in chondrocyte apoptosis. *Osteoarthritis Cartilage* 2000;8:452-63.
24. Ryu JH, Kim SJ, Chun JS, et al. Regulation of the chondrocyte phenotype by beta-catenin. *Development* 2002;129:5541-50.
25. Yu W, Gluer CC, Genant HK, et al. Influence of degenerative joint disease on spinal bone

mineral measurements in postmenopausal women. *Calcif Tissue Int* 1995;57:169-74.
26. Asai T, Ohkubo T, Katsuya T, et al. Endothelin-1 gene variant associates with blood pressure in obese Japanese subjects: the Ohasama Study. *Hypertension* 2001;38:1321-4.
27. Urano T, Shiraki M, Inoue S, et al. Association of a single-nucleotide polymorphism in low-density lipoprotein receptor-related protein 5 gene with bone mineral density. *J Bone Miner Metab* 2004;22:341-5.
28. Chapman K, Mustafa Z, Loughlin J, et al. Osteoarthritis-susceptibility locus on chromosome 11q, detected by linkage. *Am J Hum Genet* 1999;65:167-74.
29. Chapman K, Mustafa Z, Loughlin J, et al. Finer linkage mapping of primary hip osteoarthritis susceptibility on chromosome 11q in a cohort of affected female sibling pairs. *Arthritis Rheum* 2002;46:1780-3.
30. Smith AJ, Gidley J, Mansell JP, et al. Haplotypes of the low-density lipoprotein receptor-related protein 5 (LRP5) gene: are they a risk factor in osteoarthritis? *Osteoarthritis Cartilage* 2005;13:608-13.
31. Loughlin J, Dowling B, Corr M, et al. Functional variants within the secreted frizzled-related protein 3 gene are associated with hip osteoarthritis in females. *Proc Natl Acad Sci USA* 2004;101:9757-62.
32. Koay MA, Brown MA. Genetic disorders of the LRP5-Wnt signalling pathway affecting the skeleton. *Trends Mol Med* 2005;11:129-37.
33. Koh JM, Jung MH, Kim GS, et al. Association between bone mineral density and LDL receptor-related protein 5 gene polymorphisms in young Korean men. *J Korean Med Sci* 2004;19:407-12.
34. Lau HH, Ng MY, Kung AW, et al. Genetic and environmental determinants of bone mineral density in Chinese women. *Bone* 2005;36:700-9.
35. Ferrari SL, Deutsch S, Antonarakis SE, et al. Polymorphisms in the low-density lipoprotein receptor-related protein 5 (LRP5) gene are associated with variation in vertebral bone mass, vertebral bone size, and stature in whites. *Am J Hum Genet* 2004;74:866-75.
36. Mizuguchi T, Furuta I, Yoshiura K, et al. LRP5, low-density-lipoprotein-receptor-related protein 5, is a determinant for bone mineral density. *J Hum Genet* 2004;49:80-6.
37. Yamada Y, Okuizumi H, Harada A, et al. Association of transforming growth factor beta1 genotype with spinal osteophytosis in Japanese women. *Arthritis Rheum* 2000;43:452-60.
38. Hamerman D. Aging and osteoarthritis: basic mechanisms. *J Am Geriatr Soc* 1993;41:760-70.
39. Sandell LJ, Aigner T. Articular cartilage and changes in arthritis. An introduction: cell biology of osteoarthritis. *Arthritis Res* 2001;3:107-13.
40. Hwang SG, Ryu JH, Chun JS, et al. Wnt-7a Causes Loss of Differentiated Phenotype and Inhibits Apoptosis of Articular Chondrocytes via Different Mechanisms. *J Biol Chem* 2004;279:26597-604.
41. Akiyama H, Lyons JP, de Crombrugghe B, et al. Interactions between Sox9 and beta-catenin control chondrocyte differentiation. *Genes Dev* 2004;18:1072-87.

Figure legend

Figure 1. Scores of spinal osteoarthritis between the genotypes of polymorphism at Q89R (QQ vs QR + RR). (A) Scores of osteophyte formation are shown for genotype QQ and for genotype QR+RR. Scores are expressed as mean + SE. Numbers of subjects are shown in parentheses. (B) Scores of endplate sclerosis. (C) Disc space narrowing scores. The association of the two genotype groups with osteoarthritis parameters was determined by ANCOVA, a type of multifactorial analysis, with adjustment of confounding clinical variables (age, body weight, and height).

Table 1. Comparison of background, clinical characteristics between subjects bearing at least one R allele (QR + RR) and subjects with no R allele (QQ) in the *LRP5 gene coding region* (Q89R).

Items	Genotype (mean ± SD)		*P* value
	QQ	QR+RR	
Number of subjects	321	36	
Age (years)	65.0 ± 8.2	67.3 ± 8.0	NS
Height (cm)	150.7 ± 5.7	151.1 ± 7.1	NS
Body weight (kg)	50.5 ± 7.6	51.3 ± 7.9	NS
Lumber spine BMD (Z score)	-0.28 ± 1.40	-0.17 ± 1.89	NS
ALP (IU/L)	190.8 ± 61.3	194.8 ± 81.1	NS
I-OC (ng/mL)	8.2 ± 4.0	7.4 ± 3.0	NS
DPD (pmol/μmol of Cr)	7.6 ± 4.0	7.6 ± 2.3	NS
Intact PTH (pg/mL)	35.6 ± 16.7	34.6 ± 14.1	NS
1,25 $(OH)_2D_3$ (pg/ mL)	36.1 ± 10.8	37.3 ± 14.6	NS
BMI	22.1 ± 3.0	22.8 ± 3.1	NS

BMD, bone mineral density; ALP, alkaline phosphatase; I-OC, intact-osteocalcin; DPD, deoxypyridinoline; PTH, parathyroid hormone; BMI, body mass index; NS, not significant. Statistical analysis was performed according to the method described in the text.

Table 2. Association of the the *LRP5* SNP genotype with

Items	Genotype (mean ± SD)		*P* value	*P* value
	QQ	QR+RR	(un-paired t test)	(ANCOVA)
Number of subjects	321	36		
Osteopyte formation score	7.80 ± 6.51	10.89 ± 7.6	*P*=0.0083	*P*=0.0019
Endoplate scrolosis score	0.368 ± 0.845	0.389 ± 0.994	NS	NS
Disc space narrowing score	2.03 ± 1.88	2.06 ± 1.84	NS	NS

ANCOVA, Analysis of covariance.

Fig. 1.

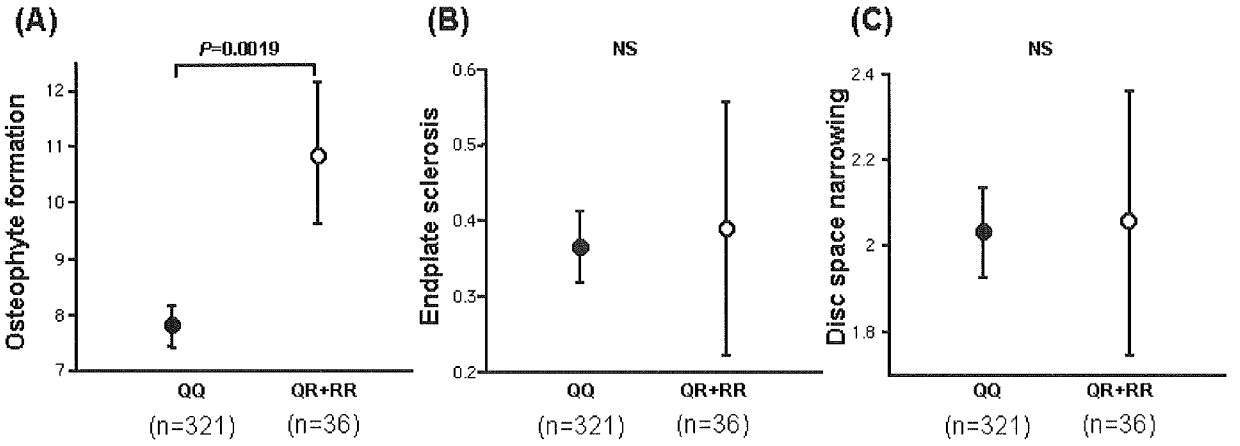
(A)
P=0.0019
Osteophyte formation
12
11
10
9
8
7
QQ
QR+RR
(n=321)
(n=36)
(B)
NS
Endplate sclerosis
0.6
0.5
0.4
0.3
0.2
QQ
QR+RR
(n=321)
(n=36)
(C)
NS
Disc space narrowing
2.4
2.2
2
1.8
QQ
QR+RR
(n=321)
(n=36)

Splicing potentiation by growth factor signals via estrogen receptor phosphorylation

Yoshikazu Masuhiro*†, Yoshihiro Mezaki*, Matomo Sakari*‡, Ken-ichi Takeyama*, Tasuku Yoshida*, Kunio Inoue§, Junn Yanagisawa*, Shigemasa Hanazawa†, Bert W. O'Malley¶, and Shigeaki Kato*‡‖

*Institute of Molecular and Cellular Biosciences, University of Tokyo, Bunkyo-ku, Tokyo 113-0032, Japan; †Division of Oral Infectious Diseases and Immunology, Faculty of Dental Science, Kyushu University, Higashi-ku, Fukuoka 812-8582, Japan; §Department of Biology, Faculty of Science, Kobe University, Nada-ku, Kobe 657-8501, Japan; ¶Department of Molecular and Cellular Biology, Baylor College of Medicine, Houston, TX 77030; and ‡Exploratory Research for Advanced Technology, Japan Science and Technology, Kawaguchi, Saitama 332-0012, Japan

Contributed by Bert W. O'Malley, April 19, 2005

Mitogen-activated protein kinase-mediated growth factor signals are known to augment the ligand-induced transactivation function of nuclear estrogen receptor α (ERα) through phosphorylation of Ser-118 within the ERα N-terminal transactivation (activation function-1) domain. We identified the spliceosome component splicing factor (SF)3a p120 as a coactivator specific for human ERα (hERα) activation function-1 that physically associated with ERα dependent on the phosphorylation state of Ser-118. SF3a p120 potentiated hERα-mediated RNA splicing, and notably, the potentiation of RNA splicing by SF3a p120 depended on hER Ser-118 phosphorylation. Thus, our findings suggest a mechanism by which growth factor signaling can regulate gene expression through the modulation of RNA splicing efficiency via phosphorylation of sequence-specific activators, after association between such activators and the spliceosome.

nuclear receptor | estrogen | coactivator | mitogen-activated protein kinase | RNA splicing

Most of the actions of estrogen are thought to be mediated via the transcriptional control of target genes by nuclear estrogen receptors (ER) α and β, members of the steroid hormone receptor gene superfamily that act as ligand-inducible transcription factors. ERs bind as dimers to specific estrogen response elements in the promoters of some target genes (1). However, most ER target promoters appear to recruit ERs without specific DNA binding, presumably through associations with sequence-specific factors bound to the promoters (2). ERs contain two transactivation functions (AFs), AF-1 in the N-terminal A/B domain and AF-2 in the C-terminal ligand-binding E/F domain. Ligand-induced transactivation by ERs requires multiple distinct classes of coactivator complexes, as well as a number of coregulators. The best-characterized complex contains p160/SRC family proteins (3, 4) and CBP/p300 histone acetyltransferases (5, 6), along with the RNA coactivator steroid receptor RNA activator (7) and presumably other known and unknown coactivators (8, 9). Another histone acetyltransferases-containing complex, the TBP-free TAF_{II}-containing (TFTC)-like complex (10), can also coactivate ER transactivation, as can the nonhistone acetyltransferases DRIP (VDR interacting protein)/TRAP (thyroid hormone receptor-associated protein)/SMCC (SRB/MED cofactor complexes)/ARC (activator-recruited cofactor) complex (11–13).

ER-mediated estrogen signaling is known to involve cross-talk with other signaling pathways (14). For instance, growth factors potentiate estrogen-induced cellular proliferation in female reproductive tissues (15). Phosphorylation of the Ser-118 residue in the human ERα (hERα) A/B domain by mitogen-activated protein kinase (MAPK) activated by growth factors (16, 17) and cyclin-dependent kinase-7 (18) results in the potentiation of AF-1 function (16). However, the molecular basis of ERα AF-1 potentiation by MAPK-mediated phosphorylation remains unclear. In a previous study, we identified the DEAD-box RNA helicase subfamily member p68/p72 as a hERα AF-1 coactivator that associated with steroid receptor RNA activator as a component in the p160/CBP histone acetyltransferases complex (19, 20). However, it appeared that the p68/p72-mediated facilitation of hERα AF-1 did not fully depend on Ser-118 phosphorylation, which suggested the presence of another, unknown factor. In the present study, we identified the spliceosome component splicing factor (SF)3a p120 as a coactivator specific for hERα AF-1 through Ser-118 phosphorylation-dependent interaction. Moreover, we found that this interaction potentiated hERα-mediated RNA splicing. Thus, our study indicated that MAPK-mediated cross-talk between growth factor and estrogen-signaling pathways modulates RNA splicing control through the phosphorylation-dependent interaction between hERα and a component of the spliceosome complex.

Materials and Methods

Plasmids and Constructs. The Pinpoint hERα (A/B) vector was prepared by inserting hERα (A/B) cDNA encoding amino acids 1–180 in-frame into HindIII/BamHI digested pinpoint Xa-3 vector (Promega). For Flag-SF3a p120 and Myc-SF3b p49 fusion constructs, respective cDNA fragments were amplified by PCR from a Marathon-Ready cDNA library (Clontech) by using pyrobest DNA polymerase (Takara, Tokyo). Myc-p68 and U1 70K cDNA were amplified by PCR, and the resultant products were digested and subcloned into pcDNA3-Flag (10), pcDNA3, and pCMV-Myc. pcDNA3-His-p72, pCMVβ-p300, pcDNA3-hERβ, pSG1-hERα, and mutants were as described (16, 20, 21). The complete coding sequences of all constructs used were verified by sequencing.

***In Vitro* Phosphorylation and Western Blotting of Biotin-Tagged hERα (A/B) Proteins.** Biotin-tagged hERα (A/B) and hERα (A/B)[S118A] proteins were expressed from Pinpoint Xa-3 vectors in *Escherichia coli* HB101, purified on avidin resin, and eluted with free biotin according to the manufacturer's protocol (Promega). To determine the efficiency of hERα (A/B) domain Ser-118 residue phosphorylation by MAPK *in vitro*, purified proteins and 50 ng of myelin basic protein (MBP) (Sigma) were coincubated for 30 min with MAPK (Erk2, New England Biolabs) in a total volume of 25 μl. Phosphorylated proteins were analyzed by 12.5% SDS/PAGE and autoradiography. Biotinylation of purified hERα (A/B) proteins was confirmed by Western blotting by using conjugated streptavidin-alkaline phosphatase (Promega).

Abbreviations: ERα, estrogen receptor α; hER, human ER; E2, 17β-estradiol; AF, transactivation function; TAM, 4-hydroxy-tamoxifen; SF, splicing factor; snRNP, small nuclear ribonucleoprotein particle; MAPK, mitogen-activated protein kinase; siRNA, short interfering RNA.

‖To whom correspondence should be addressed. E-mail: uskato@mail.ecc.u-tokyo.ac.jp.

www.pnas.org/cgi/doi/10.1073/pnas.0503197102

Far-Western Blotting and Expression Cloning. To detect endogenous interactants for phosphorylated Ser-118 hERα (A/B) domains, nuclear extracts from HeLa, COS-1, and MCF7 cells were prepared, and 10-μg aliquots of each nuclear extract were boiled and loaded onto 7.5% SDS/PAGE gels. Proteins were transferred onto poly(vinylidene difluoride) membranes and denatured in 6 M guanidine hydrochloride, 50 mM Tris·HCl (pH 8.0), 5 mM 2-mercaptoethanol, and 0.05% Tween 20 for 1 h at room temperature. Immobilized proteins were renatured overnight at 4°C. Membranes were rinsed and incubated with phosphorylated and biotin-tagged hERα (A/B) probe (0.1 μg/ml) for 4 h at room temperature. Membranes were washed and hybridization products detected by using conjugated streptavidin-alkaline phosphatase.

For expression cloning, a human kidney cDNA library in the Zap II vector was infected into bacteria, plated, and incubated at 42°C until minute plaques were seen. Recombinant plaques were grown at 37°C for 4 h and then induced with 1 mM isopropyl β-D-thiogalactoside-impregnated nitrocellulose filters for 3.5 h. Filters were then treated under the same conditions as for Far-Western blotting for denaturation and detection. Positive plaques were isolated, amplified, and processed, with the procedure repeated until 100% of the plaques were positive after plating. Four rounds of screening were performed after which cDNA inserts from plaques were obtained as pBluescript plasmids by *in vivo* excision. Isolated clones were sequenced by using T7 primers on an Applied Biosystems automatic sequencer.

Protein Identification by MALDI-TOF MS. Protein bands in SDS/PAGE gels were excised and digested in-gel with trypsin. Eluted peptides were then loaded onto the sampling plate for MALDI-TOF MS (Voyager DE-STR, Perseptive Biosystems). After analysis of each protein fragment mass, results were compared by using the MS-FIT program (University of California, San Francisco Mass Spectrometry Facility).

Pull-Down Assay. GST-fused proteins were expressed in *E. coli* and purified on glutathione-Sepharose beads (Amersham Pharmacia). Pull-down assays were performed as described (10, 16, 19–21). Immobilized glutathione-Sepharose and avidin-resin were incubated with ^{35}S-methionine-labeled SF3a p120 protein. Bound proteins were eluted and analyzed by 7.5% SDS/PAGE.

Splicing Assay. The 293T cells were transfected with reporter CD44 minigene (22), pCH110 internal control plasmid containing β-galactosidase (10 ng), short-interfering RNA (siRNA), and expression plasmids as indicated. Total RNA was isolated by Isogen (Nippon Gene, Toyama, Japan), and RT-PCR for CD44 was performed as described (22). For oxytocin, total RNA (0.1 μg) was reverse-transcribed in 50-μl reaction mixtures by using the Access RT-PCR system (Promega) with primers specific for oxytocin (reverse, 5′-CAGGTAGTTCTCCTCCTGGCAGC-3′) or β-galactosidase (reverse, 5′-CCGCCGATACTGACGGGCTCC-3′). PCR was then performed by using 3 μl of this mixture in a 50-μl reaction volume containing 0.5 unit of ExTaqDNA polymerase (Takara) and gene-specific primers for oxytocin (forward, 5′-CAGCCTCGCTTGCTGTCTGCTC-3′; reverse, 5′-CAGGTAGTTCTCCTCCTGGCAGC-3′) or β-galactosidase (forward, 5′-CGACCGCTCACGCGTGGCAGC-3′; reverse, 5′-CCGCCGATACTGACGGGCTCC-3′). PCR conditions were optimized to allow semiquantitative measurement of oxytocin (denaturation at 96°C for 1 min followed by 25–30 cycles of 96°C for 20 s, 70°C for 20 s, and 72°C for 1 min) and β-galactosidase (denaturation at 96°C for 1 min followed by 20–25 cycles of 96°C for 20 s, 70°C for 20 s, and 72°C for 1 min) mRNA levels. PCR products were verified by sequencing and visualized on 2% agarose/Tris-acetate-EDTA gels. Quantitative measurement of splicing efficiency was analyzed by NIH IMAGE (National Institutes of Health, Bethesda).

Chromatin Immunoprecipitation Assay. Chromatin immunoprecipitation assays for oxytocin were performed as described (10, 23). Soluble chromatin from MCF7 cells was immunoprecipitated with Abs against the indicated proteins. Specific primer pairs used to PCR amplify oxytocin were 5′-CACCCTAGTGGCCCAGGCCACC-3′ and 5′-GCTCTGTTTAAGAGGTTGGTAGTATG-3′. PCR conditions were optimized to allow semiquantitative measurement. Conditions used were 21–25 cycles of 20 s at 96°C, 20 s at 70°C, and 1 min at 72°C. PCR products were visualized on 2% agarose/Tris-acetate-EDTA gels.

Results and Discussion

Identification of SF3a p120 as a Direct Interactant for hERα Phosphorylated by MAPK at Ser-118. To identify the factor fully responsible for the phosphorylation-dependent potentiation of hERα AF-1, we performed Far-Western blot analysis on nuclear extracts by using bacterially expressed biotinylated hERα (A/B) domains as a probe. hERα (A/B) domains, phosphorylated *in vitro* by MAPK, detected three endogenous proteins with approximate M_r of 120, 72, and 68 kDa in nuclear extracts from the HeLa, COS-1, and MCF7 cell lines (Fig. 1*A Center*, lanes 5–7). As the 68- and 72-kDa bands corresponded to p68/p72 (19, 20) by Western blotting with specific Abs (data not shown), we attempted to clone the p120 factor by Far-Western screening of a human kidney cDNA library because ERα AF-1 activity is high in the kidney. Screening of 8×10^6 independent clones yielded 72 positives, three of which encoded overlapping cDNA sequences that corresponded to the C-terminal domain of SF3a p120 (24, 25). Biochemical purification of interactants from stably expressed hERα (Fig. 1*B Right*) and phosphorylated hERα A/B domains fused to GST [GST-*p*-Ser-118 hERα (A/B)] (Fig. 1*B Left*, lane 5) followed by MS (MALDI-TOF MS) confirmed the identity of the three isolated proteins as SF3a p120 and p68/p72. No such association was detected by using a hERα mutant that cannot be phosphorylated by MAPK because of the substitution of the Ser-118 residue with Ala [S118A (16) (Fig. 1*B*, *Right*)].

We then tested whether SF3a p120 directly bound the A/B or E/F domains of hERα or hERβ by using an *in vitro* GST pull-down assay (10). Unlike p68/p72 (19, 20), SF3a p120 exhibited a strict association only with A/B domains from phosphorylated Ser-118 hERα and Glu-118 hERα (S118E), a transcriptionally dominant active mutant with Ser-118 substituted with Glu to mimic the negative charge of phosphorylated Ser-118 (Fig. 1*C*, lanes 4 and 5). In contrast, SF3a p120 did not interact with the Ser-118–Ala mutant (Fig. 1*C*, lane 3), the E/F domain of ERα, or ERβ A/B or D/E/F domains (see Fig. 1*C*, lanes 7–11). We then tested whether SF3a p120 directly associated with hERα *in vivo* by using immunoprecipitation assays on 293T cells. The *in vivo* association between SF3a p120 and full-length hERα depended on ligand binding and was abrogated by both the MAPK inhibitor U0126 (Fig. 2*A*, compare lanes 6 and 7) and the Ser-118–Ala mutant (Fig. 2*A*, lanes 8–10). As expected from the coimmunoprecipitation assay results (Fig. 2*A*), activation of MAPK signaling by EGF treatment potentiated the association of hERα with endogenous SF3a p120 in MCF7 cells (Fig. 2*B*, lane 3). As the hERα AF-1 domain (hERα A/B/C) alone appeared to be sufficient for association with SF3a p120 (Fig. 2*A*, lane 12), it is possible that the structural alterations in ERα induced by ligand binding expose the functional AF-1 domain, rendering it accessible to SF3a p120.

SF3a p120 Is a Coactivator for Ser-118 Phosphorylated hERα AF-1. As SF3a p120 appeared to physically interact with the hERα AF-1 domain, we tested the coregulatory function of SF3a p120 in a

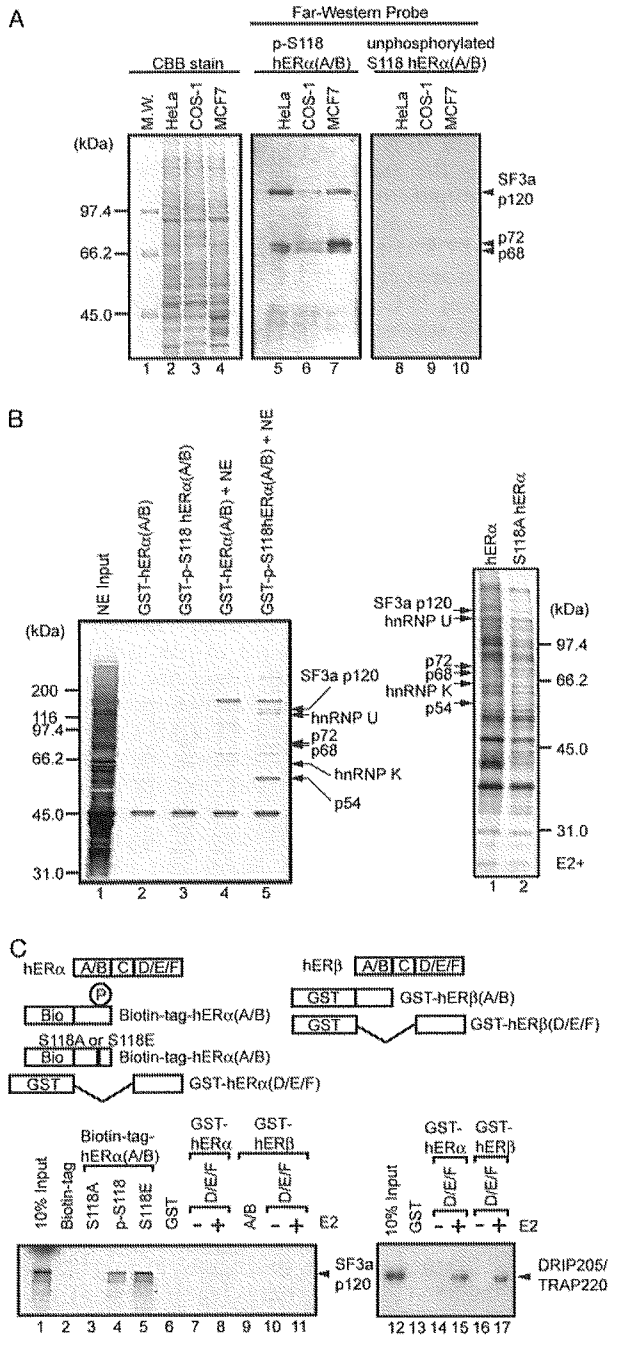

Fig. 1. SF3a p120 directly binds phosphorylated Ser-118 hERα (A/B) domains. (*A*) Endogenous interactants of the hERα (A/B) domain. Three endogenous interactants (p120, p72, and p68, as indicated) were detected in 10 μg of nuclear extracts from HeLa, COS-1, and MCF7 cells lines with Ser-118 phosphorylated or nonphosphorylated hERα (A/B) domain probes by using the Far-Western technique (20). (*Left*) Coomassie brilliant blue R-250 (CBB)-stained gel. (*B*) Identification of phosphorylated hERα (A/B) domain-interacting proteins. Nuclear extracts prepared from HeLa S3 cells were incubated with immobilized GST-hERα (A/B) or GST-*p*-Ser-118 hERα (A/B) domains. (*Left*) Proteins eluted from the columns by 1 M KCl were subjected to SDS/PAGE followed by staining with CBB. (*Right*) Products of FLAG-M2 resin affinity purification from nuclear extracts of HeLa cells stably expressing FLAG-hERα or FLAG-Ser-118–Ala hERα were examined by MS. Identified proteins are indicated at the right. (*C*) Selective binding of SF3a p120 to hERα in a pull-down assay. *In vitro*-translated SF3a p120 protein was tested for direct interaction with biotin-tagged hERα (A/B), chimeric GST-fused A/B domain of hERβ, or D/E/F domains of hERα or hERβ. DRIP205/TRAP220 was used as a positive control and exhibited ligand-induced association with the hERα D/E/F domain.

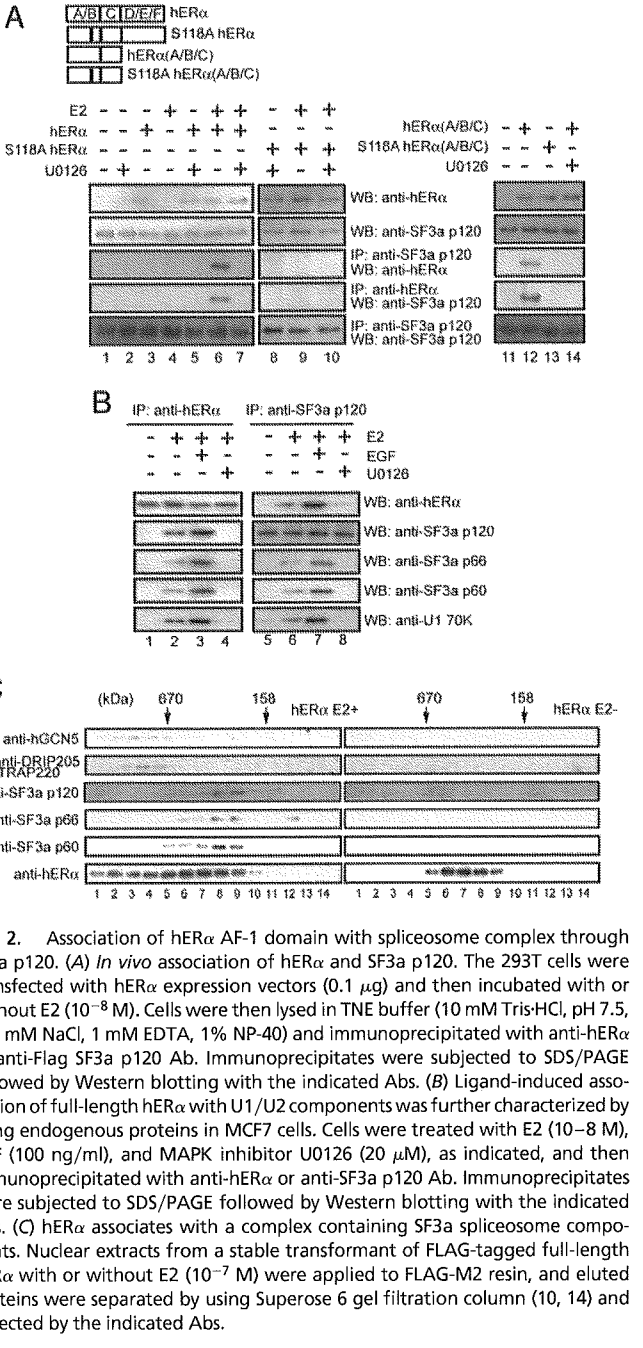

Fig. 2. Association of hERα AF-1 domain with spliceosome complex through SF3a p120. (*A*) *In vivo* association of hERα and SF3a p120. The 293T cells were transfected with hERα expression vectors (0.1 μg) and then incubated with or without E2 (10^{-8} M). Cells were then lysed in TNE buffer (10 mM Tris·HCl, pH 7.5, 150 mM NaCl, 1 mM EDTA, 1% NP-40) and immunoprecipitated with anti-hERα or anti-Flag SF3a p120 Ab. Immunoprecipitates were subjected to SDS/PAGE followed by Western blotting with the indicated Abs. (*B*) Ligand-induced association of full-length hERα with U1/U2 components was further characterized by using endogenous proteins in MCF7 cells. Cells were treated with E2 (10^{-8} M), EGF (100 ng/ml), and MAPK inhibitor U0126 (20 μM), as indicated, and then immunoprecipitated with anti-hERα or anti-SF3a p120 Ab. Immunoprecipitates were subjected to SDS/PAGE followed by Western blotting with the indicated Abs. (*C*) hERα associates with a complex containing SF3a spliceosome components. Nuclear extracts from a stable transformant of FLAG-tagged full-length hERα with or without E2 (10^{-7} M) were applied to FLAG-M2 resin, and eluted proteins were separated by using Superose 6 gel filtration column (10, 14) and detected by the indicated Abs.

transient transfection experiment by using a luciferase reporter plasmid bearing estrogen response elements (10, 20) transfected into 293T cells. Although SF3a p120 enhanced the estrogen-induced transactivation function of full-length hERα (Fig. 3*A*, lane 5), with a 2- to 3-fold increase in hERα (A/B/C) AF-1 activity (Fig. 3*B*, lane 5), no potentiation of AF-2 activity of hERα (D/E/F) was observed (data not shown). Introduction of SF3a p120 siRNA significantly lowered the ligand-induced transactivation of hERα and dramatically attenuated MAPK signaling-induced potentiation (Fig. 3*A*, lanes 6, 9, and 12). To examine the AF-1-specific coactivator function of SF3a p120 for full-length hERα, we tested SF3a p120 activity on hERα bound to 4-hydroxy-tamoxifen (TAM), an AF-1 agonist/AF-2 antagonist (16). As expected, partial transactivation of TAM-bound ERα was observed, presumably via activated AF-1 (Fig. 3*A*, lanes 19–27). This transactivation was potentiated by both SF3a p120

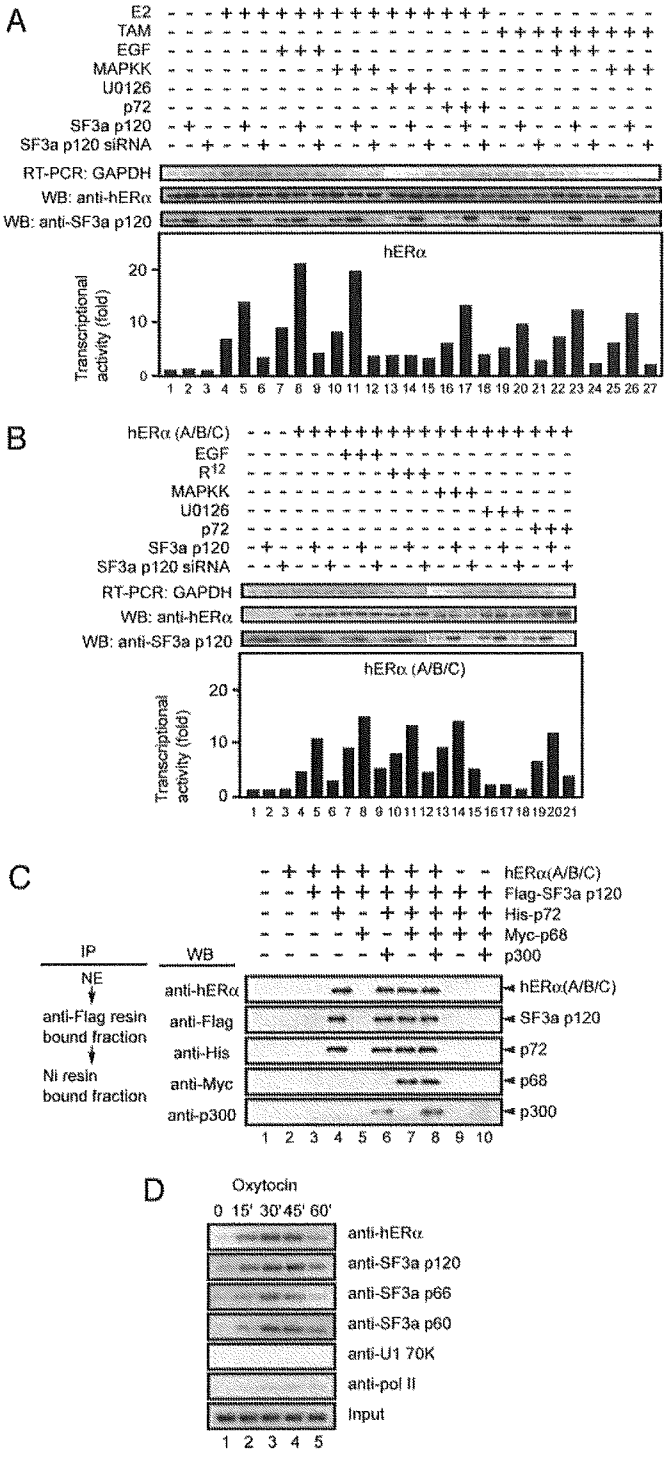

Fig. 3. SF3a p120 coactivates the transactivation function of hERα AF-1. (*A* and *B*) SF3a p120 potentiates the transactivation function of hERα AF-1 in a Ser-118 phosphorylation-dependent manner. The 293T cells were transfected with expression vectors of full-length hERα (50 ng), hERα (A/B/C) (50 ng), Ki-Ras^{val12} (R^{12}) (100 ng), MAPKK (100 ng), SF3a p120 (300 ng), or combinations as indicated, in either the absence or presence of E2 (10^{-8} M), TAM (10^{-7} M), U0126 (20 μM), or combinations as indicated, along with pGL-estrogen response element-tk (1.0 μg) and pRL-CMV (10 ng). Cultured cells were also transfected with 100 pmol dsRNA for SF3a p120 siRNA (5′-AGACGGAAUGGAAACUGAAUGGGCAAG-3′ and 5′-UGCCCAUUCAGUUUCCAUUCCGUCUAU-3′) by using Lipofectamine 2000 (Invitrogen). Assays were performed 24 h after transfection. (*Upper*) Cell extracts were used in luciferase assays (20) and Western blotting. (*C*) SF3a p120 enhances the association of hERα AF-1 with p68, p72, and p300. The 293T cells were transfected with indicated plasmids. The complex associated with A/B/C domains of hERα were analyzed to detect SF3a p120, p68, p72, and p300 by purification from the cell extracts with anti-Flag M2 resin and Ni resin, followed by Western blotting by using the anti-hERα, anti-Flag, anti-His, anti-Myc, or anti-p300 Abs (lanes 1–10). (*D*) Occupancy of human oxytocin promoter by hERα and spliceosome components in MCF7 cells was determined by chromatin immunoprecipitation analysis (14, 23).

and MAPK activators, with the simultaneous addition of MAPK activators and SF3a p120 resulting in additive potentiation (Fig. 3*A*, compare lane 19 and lanes 20, 23, and 26). To further examine the SF3a p120 hERα AF-1 coactivator function, possible interaction with known hERα AF-1 coactivators was tested by coimmunoprecipitation by using SF3a p120. p68/p72 and p300 were detected in the SF3a p120 coimmunoprecipitants (data not shown), and we then verified these associations by further testing the complexes that formed around the hERα AF-1 domain (Fig. 3*C*). Purification of the SF3a p120-containing complex that associated with hERα (A/B/C) by using sequential affinity columns identified p68/72 and p300, which raised the hypothesis that SF3a p120 was the associating component of the p68/72 and p300 hERα AF-1 coactivator complex (20).

To examine these *in vivo* associations, we performed a chromatin immunoprecipitation assay by using full-length hERα in MCF7 cells, spliceosome complex components, and a gene promoter region from human oxytocin that contained an estrogen-responsive element (26). Upon 17β-estradiol (E2) stimulation, the SF3a subunits and hERα all were recruited to the oxytocin promoter along with RNA polymerase II (Fig. 3*D*).

Phosphorylated hERα Associates with the Spliceosome Through SF3a p120. Because SF3a p120 is known to be a component of U2 small nuclear ribonucleoprotein particle, which forms the spliceosome along with the U1 complex (24, 25), we used coimmunoprecipitation to determine whether phosphorylated hERα associated with the spliceosome via SF3a p120. Coimmunoprecipitation experiments were performed with extracts from hERα-expressing MCF7 cells, and results indicated that all U1/U2 endogenous components tested (U2: SF3a p66, SF3a p60 small nuclear ribonucleoprotein particles; and U1: U1 70K small nuclear ribonucleoprotein particles) (27, 28) were coimmunoprecipitated with endogenous hERα, with these associations potentiated by EGF treatment (Fig. 2*B*, lanes 1–4). Similar results were obtained by using anti-SF3a p120 (Fig. 2*B*, lanes 5–8). Moreover, the U2 components were detected as a single complex by Western blotting after liganded hERα-associated complexes were biochemically isolated from HeLa nuclear extracts and fractionated by gel filtration (10, 14, 29) (Fig. 2*C Left*, lanes 8 and 9).

SF3a p120 Potentiates hERα-Mediated RNA Splicing. To test whether the phosphorylation-dependent association of hERα with spliceosome components modulated mRNA processing, we examined the effect of SF3a p120 on RNA splicing by using a test CD44 minigene, as reported (Fig. 4*A*) (22). Although estrogen (E2) stimulated transcription via hERα or hERβ (Fig. 4*B*, lanes 6 and 12), the ratio of skipped to unskipped transcripts was enhanced only by liganded ERα. SF3a p120 clearly potentiated hERα-mediated RNA splicing (Fig. 4*B*, lane 7). Unlike SF3a p120, neither p68 nor p72 was able to potentiate intron excision. Indeed, p68/p72 inhibited exon skipping in the CD44 minigene (Fig. 4*B*, lane 8), as expected from previous studies (22, 30), despite the finding that p68/p72 coactivated ERα-mediated transcription (see Fig. 3*A*, lane 16–18, for p72 activity as a representative of p68/p72) (19, 20). Similar results were observed by using a human β-globin minigene and a mutant ERα AF-1 domain fused to the yeast GAL4-DNA binding domain. In

BIOCHEMISTRY

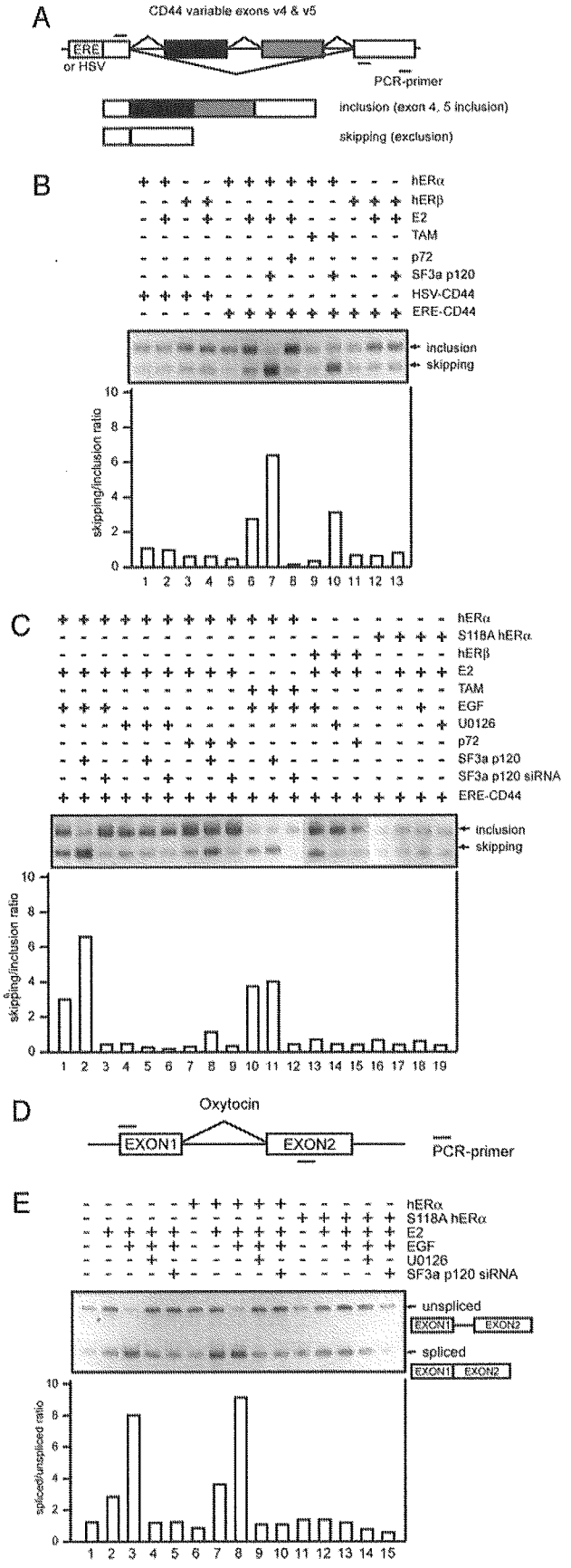

Fig. 4. hERα AF-1-specific potentiation of mRNA processing by SF3a p120. (*A*) Schematic representation of the estrogen response element-CD44 construct used in the *in vivo* splicing assay (22). (*B* and *C*) SF3a p120 regulation of CD44 mRNA processing depends on hERα Ser-118 phosphorylation state. The 293T cells were transfected with the indicated plasmids and siRNA (SF3a p120; 100 pmol). After transfection, cells were treated with E2 (10−8 M), TAM (10−7 M), EGF (100 ng/ml), and U0126 (20 μM) as indicated. Total RNA was extracted with Isogen 24 h after transfection and subjected to RT-PCR analysis (22). (*D*) Schematic representation of the human oxytocin gene exon 1 and 2 used in the *in vivo* splicing assay. (*E*) MCF7 cells were transfected with the indicated plasmids and treated as in *B* and *C*. After the treatment, total RNA was extracted. Splicing patterns were evaluated by RT-PCR by using oxytocin-specific primers.

that system, the hERα AF-1 domain alone was able to potentiate RNA splicing (data not shown).

RNA Splicing Augmented by hERα Depends on hERα Ser-118 Phosphorylation by MAPK. Reflecting the Ser-118 phosphorylation-dependent association between hERα and SF3a p120 (Fig. 2*A*), both Ala substitution in the AF-1 domain (S118A) (Fig. 4*C*, lanes 16–19) and SF3a p120 siRNA (Fig. 4*C*, lanes 3, 6, and 9) abrogated the potentiation of intron excision by hERα. The efficiency of RNA splicing from the CD44 minigene mediated by hERα appeared to depend on SF3a p120 expression level and activated MAPK signaling via EGF treatment (Fig. 4*C*, compare lanes 1 and 4). TAM treatment (20) further confirmed the AF-1 specificity of SF3a p120 on hERα (Fig. 4*B*, compare lanes 9 and 10). Neither potentiation of exon skipping by SF3a p120 nor increased RNA splicing caused by activated MAPK was observed for the full-length hERα Ser-118–Ala mutant (Fig. 4*C*, lanes 16–19). Reflecting the phosphorylation-dependent association of SF3a p120 with hERα through the A/B AF-1 domain, activation of MAPK by Ki-Ras^{val12}, MAPKK, or EGF also potentiated the effects of SF3a p120 on RNA splicing mediated by the hERα A/B-AF-1 domain alone (data not shown). Such potentiation via activated MAPK signaling was not detectable in the hERα Ser-118–Ala mutant A/β-GAL-DNA binding domain (data not shown). Notably, neither a significant increase in spliced transcript stability nor specific intracellular localization was observed when transcription was potentiated under any of the conditions tested (data not shown).

Finally, to address the physiological relevance of our findings, we screened several known endogenous ERα target genes that show ERα-regulated splicing. We found that the human oxytocin gene generated a transcript that retained intron 1 sequence (see Fig. 4*D*). In response to E2 treatment, intron 1 splicing was increased along with enhanced transcription in MCF7 cells (Fig. 4*E*, compare lanes 1 and 2). EGF-mediated MAPK activation further enhanced RNA splicing mediated by hERα (Fig. 4*E*, lanes 3 and 8). However, Ser-118–Ala hERα expression abrogated this increase in RNA splicing after EGF treatment (Fig. 4*E*, lane 13). Thus, our findings suggested that the potentiation of splicing efficiency mediated via the association of phosphorylated hERα with SF3a p120 occurred in at least some hERα target genes.

Cross-Talk Between Estrogen and Growth Factor Signaling Mediates the Control of RNA Splicing. Our study uncovered a unique mechanism by which RNA splicing is potentiated by MAPK-mediated growth factor signaling through Ser-118 phosphorylation of hERα, such that augmented RNA splicing may, at least in part, account for the effects of SF3a p120 coactivation on the ligand-induced transactivation functions of hERα. Based on our findings, it is also possible that phosphorylated, but DNA-unbound, hERα may serve as a coregulator of RNA splicing in some estrogen-responsive gene promoters. Recent reports have shown that the RNA splicing process is coupled with transcriptional events under the control of sequence-specific activators, such as peroxisome proliferator-activated

receptor (PPAR)γ and steroid receptors (22, 30–35). Thus, given the current view that the progression from transcription to splicing is a sequential, yet rapid process (36), it is likely that the spliceosome functionally associates, directly or indirectly, with activator molecules, presumably including coregulators and transcription elongation factors. The efficiency of RNA splicing is then modulated via the association between transcription-related factors and the spliceosome. The present study provides an example of coordinated regulation of transcription and intron excision modulated by growth factor signaling via the association of an activator with the spliceosome. This mechanism may support, at least in part, growth factor-mediated gene regulation.

We thank Dr. C. Will (Max Planck Institute, Gottingen, Germany) for the kind gift of the U1 70K plasmid; Drs. M. Saitoh, K. Goto, and H. Nawata for technical help; Drs. P. Chambon, D. Metzger, and H. Kawate for helpful suggestions and plasmids; and H. Higuchi for manuscript preparation. This work was supported in part by the Program for Promotion of Basic Research Activities for Innovative Biosciences and priority areas from the Ministry of Education, Science, Sports and Culture of Japan (to S.K.) and National Institutes of Health Grant 08818 (to B.W.O.).

1. Parker, M. G. (1998) *Biochem. Soc. Symp.* **63,** 45–50.
2. Kushner, P. J., Agard, D. A., Greene, G. L., Scanlan, T. S., Shiau, A. K., Uht, R. M. & Webb, P. (2000) *J. Steroid Biochem. Mol. Biol.* **74,** 311–317.
3. Onate, S. A., Tsai, S. Y., Tsai, M. J. & O'Malley, B. W. (1995) *Science* **270,** 1354–1357.
4. Chen, H., Lin, R. J., Schiltz, R. L., Chakravarti, D., Nash, A., Nagy, L., Privalsky, M. L., Nakatani, Y. & Evans, R. M. (1997) *Cell* **90,** 569–580.
5. Kamei, Y., Xu, L., Heinzel, T., Torchia, J., Kurokawa, R., Gloss, B., Lin, S. C., Heyman, R. A., Rose, D. W., Glass, C. K., *et al.* (1996) *Cell* **85,** 403–414.
6. Spencer, T. E., Jenster, G., Burcin, M. M., Allis, C. D., Zhou, J., Mizzen, C. A., McKenna, N. J., Onate, S. A., Tsai, S. Y., Tsai, M. J., *et al.* (1997) *Nature* **389,** 194–198.
7. Lanz, R. B., McKenna, N. J., Onate, S. A., Albrecht, U., Wong, J., Tsai, S. Y., Tsai, M. J. & O'Malley, B. W. (1999) *Cell* **97,** 17–27.
8. McKenna, N. J. & O'Malley, B. W. (2002) *Cell* **108,** 465–474.
9. Spiegelman, B. M. & Heinrich, R. (2004) *Cell* **119,** 157–167.
10. Yanagisawa, J., Kitagawa, H., Yanagida, M., Wada, O., Ogawa, S., Nakagomi, M., Oishi, H., Yamamoto, Y., Nagasawa, H., McMahon, S. B., *et al.* (2002) *Mol. Cell* **9,** 553–562.
11. Fondell, J. D., Ge, H. & Roeder, R. G. (1996) *Proc. Natl. Acad. Sci. USA* **93,** 8329–8333.
12. Rachez, C., Lemon, B. D., Suldan, Z., Bromleigh, V., Gamble, M., Naar, A. M., Erdjument-Bromage, H., Tempst, P. & Freedman, L. P. (1999) *Nature* **398,** 824–828.
13. Naar, A. M., Beaurang, P. A., Zhou, S., Abraham, S., Solomon, W. & Tjian, R. (1999) *Nature* **398,** 828–832.
14. Ohtake, F., Takeyama, K., Matsumoto, T., Kitagawa, H., Yamamoto, Y., Nohara, K., Tohyama, C., Krust, A., Mimura, J., Chambon, P., *et al.* (2003) *Nature* **423,** 545–550.
15. Couse, J. F. & Korach, K. S. (1999) *Endocr. Rev.* **20,** 358–417.
16. Kato, S., Endoh, H., Masuhiro, Y., Kitamoto, T., Uchiyama, S., Sasaki, H., Masushige, S., Gotoh, Y., Nishida, E., Kawashima, H., *et al.* (1995) *Science* **270,** 1491–1494.
17. Feng, W., Webb, P., Nguyen, P., Liu, X., Li, J., Karin, M. & Kushner, P. J. (2001) *Mol. Endocrinol.* **15,** 32–45.
18. Chen, D., Riedl, T., Washbrook, E., Pace, P. E., Coombes, R. C., Egly, J. M. & Ali, S. (2000) *Mol. Cell* **6,** 127–137.
19. Endoh, H., Maruyama, K., Masuhiro, Y., Kobayashi, Y., Goto, M., Tai, H., Yanagisawa, J., Metzger, D., Hashimoto, S. & Kato, S. (1999) *Mol. Cell. Biol.* **19,** 5363–5372.
20. Watanabe, M., Yanagisawa, J., Kitagawa, H., Takeyama, K., Ogawa, S., Arao, Y., Suzawa, M., Kobayashi, Y., Yano, T., Yoshikawa, H., *et al.* (2001) *EMBO J.* **20,** 1341–1352.
21. Kobayashi, Y., Kitamoto, T., Masuhiro, Y., Watanabe, M., Kase, T., Metzger, D., Yanagisawa, J. & Kato, S. (2000) *J. Biol. Chem.* **275,** 15645–15651.
22. Auboeuf, D., Honig, A., Berget, S. M. & O'Malley, B. W. (2002) *Science* **298,** 416–419.
23. Shang, Y., Hu, X., DiRenzo, J., Lazar, M. A. & Brown, M. (2000) *Cell* **103,** 843–852.
24. Brosi, R., Groning, K., Behrens, S. E., Luhrmann, R. & Kramer, A. (1993) *Science* **262,** 102–105.
25. Brosi, R., Hauri, H. P. & Kramer, A. (1993) *J. Biol. Chem.* **268,** 17640–17646.
26. Stedronsky, K., Telgmann, R., Tillmann, G., Walther, N. & Ivell, R. (2002) *J. Neuroendocrinol.* **14,** 472–485.
27. Nilsen, T. W. (2003) *BioEssays* **25,** 1147–1149.
28. Soret, J. & Tazi, J. (2003) *Prog. Mol. Subcell. Biol.* **31,** 89–126.
29. Kitagawa, H., Fujiki, R., Yoshimura, K., Mezaki, Y., Uematsu, Y., Matsui, D., Ogawa, S., Unno, K., Okubo, M., Tokita, A., *et al.* (2003) *Cell* **113,** 905–917.
30. Cramer, P., Caceres, J. F., Cazalla, D., Kadener, S., Muro, A. F., Baralle, F. E. & Kornblihtt, A. R. (1999) *Mol. Cell* **4,** 251–258.
31. Monsalve, M., Wu, Z., Adelmant, G., Puigserver, P., Fan, M. & Spiegelman, B. M. (2000) *Mol. Cell* **6,** 307–316.
32. Iwasaki, T., Chin, W. W. & Ko, L. (2001) *J. Biol. Chem.* **276,** 33375–33383.
33. Zhao, Y., Goto, K., Saitoh, M., Yanase, T., Nomura, M., Okabe, T., Takayanagi, R. & Nawata, H. (2002) *J. Biol. Chem.* **277,** 30031–30039.
34. Brand, M., Moggs, J. G., Oulad-Abdelghani, M., Lejeune, F., Dilworth, F. J., Stevenin, J., Almouzni, G. & Tora, L. (2001) *EMBO J.* **20,** 3187–3196.
35. Honig, A., Auboeuf, D., Parker, M. M., O'Malley, B. W. & Berget, S. M. (2002) *Mol. Cell. Biol.* **22,** 5698–5707.
36. Orphanides, G. & Reinberg, D. (2002) *Cell* **108,** 439–451.

nature medicine

Impaired flow-dependent control of vascular tone and remodeling in P2X4-deficient mice

Kimiko Yamamoto[1,6], Takaaki Sokabe[1,6], Takahiro Matsumoto[2], Kimihiro Yoshimura[2], Masahiro Shibata[1], Norihiko Ohura[1], Toru Fukuda[2], Takashi Sato[2], Keisuke Sekine[2], Shigeaki Kato[2], Masashi Isshiki[3], Toshiro Fujita[3], Mikio Kobayashi[4], Koichi Kawamura[4], Hirotake Masuda[4], Akira Kamiya[5] & Joji Ando[1]

The structure and function of blood vessels adapt to environmental changes such as physical development and exercise[1–3]. This phenomenon is based on the ability of the endothelial cells to sense and respond to blood flow[4–6]; however, the underlying mechanisms remain unclear. Here we show that the ATP-gated P2X4 ion channel[7,8], expressed on endothelial cells and encoded by *P2rx4* in mice, has a key role in the response of endothelial cells to changes in blood flow. *P2rx4*$^{-/-}$ mice do not have normal endothelial cell responses to flow, such as influx of Ca^{2+} and subsequent production of the potent vasodilator nitric oxide (NO). Additionally, vessel dilation induced by acute increases in blood flow is markedly suppressed in *P2rx4*$^{-/-}$ mice. Furthermore, *P2rx4*$^{-/-}$ mice have higher blood pressure and excrete smaller amounts of NO products in their urine than do wild-type mice. Moreover, no adaptive vascular remodeling, that is, a decrease in vessel size in response to a chronic decrease in blood flow, was observed in *P2rx4*$^{-/-}$ mice. Thus, endothelial P2X4 channels are crucial to flow-sensitive mechanisms that regulate blood pressure and vascular remodeling.

P2X-type ATP receptors are distributed throughout the entire body and are involved in the regulation of the physiological function of many tissues and organs[7]. When ATP binds to P2X receptors on the surface of cells, extracellular Ca^{2+} enters and activates signal transduction pathways that evoke a variety of cellular responses. Thus far, seven P2X subtypes, P2X1–7, have been cloned; all of them contain two transmembrane domains and function as cation channels in the form of hetero- or homo-oligomers[8]. An immunohistochemical analysis in rats has shown that P2X4 receptors are widely distributed in the central and peripheral nervous systems, the epithelium of exocrine glands and the airway, bladder smooth muscle, the gastrointestinal tract, uterus, arteries and adipose cells[9]. Recent studies including ours have shown that P2X4 is the most abundantly expressed P2X receptor subtype in vascular endothelial cells[10–12] and is the major contributor to ATP- and flow-induced Ca^{2+} influx in endothelial cells[13].

Endothelial cells are in direct contact with blood flow and are exposed to shear stress, the frictional force exerted by flowing blood. A number of recent studies have shown that endothelial cells recognize changes in shear stress and transmit signals to the interior of the cell, which leads to cellular responses that involve changes in cell morphology, cell function and gene expression[5]. These endothelial cell responses to shear stress are thought to have important roles in blood flow–dependent phenomena, such as control of vascular tone, angiogenesis, vascular remodeling and atherogenesis. Ca^{2+} signaling has an important role in shear-stress signal transduction; it has been shown that a shear stress–dependent Ca^{2+} influx occurs in bovine and human endothelial cells when exposed to flow in the presence of extracellular ATP[10,14], and treatment of endothelial cells with antisense oligonucleotides designed to knock down expression of *P2RX4* abolishes the shear stress–dependent Ca^{2+} influx[13]. Human embryonic kidney 293 cells do not exhibit a Ca^{2+} response to flow, but when transfected with *P2RX4* cDNA, they express P2X4 receptors and exhibit shear stress–dependent Ca^{2+} influx[13]. These findings suggest that P2X4 receptors have a 'shear-transducer' property through which shear stress signals are transmitted into the cell interior through influx of Ca^{2+}. It has also been shown that endothelial cells release ATP in response to shear stress[15], but the physiological and pathological significance of this shear-sensing mechanism through ATP and its receptors is not fully understood. To gain insight into its significance, we generated *P2rx4*-deficient mice using embryonic stem cells (**Supplementary Fig. 1** online).

Northern blot analysis in *P2rx4*$^{-/-}$ mice detected no *P2rx4* mRNA in pulmonary microvessel endothelial cells, confirming inactivation of *P2rx4* (**Fig. 1a**). Comparison of levels of mRNA encoding P2X subtypes by a competitive PCR method showed that P2X4 was the most strongly expressed isoform in endothelial cells of wild-type mice, but was absent in endothelial cells of *P2rx4*$^{-/-}$ mice (**Fig. 1b**). No compensatory upregulation of any subtypes occurred in the endothelial cells of *P2rx4*$^{-/-}$ mice. The absence of the P2X4 receptor in endothelial cells of *P2rx4*$^{-/-}$ mice was also confirmed at the protein level. A P2X4-specific antibody showed high levels of immunoreactivity in

[1]Department of Biomedical Engineering, Graduate School of Medicine, University of Tokyo, Tokyo 113-0033, Japan. [2]Institute of Molecular and Cellular Biosciences, University of Tokyo, Tokyo 113-0032, Japan. [3]Department of Nephrology and Endocrinology, Graduate School of Medicine, University of Tokyo, Tokyo 113-8655, Japan. [4]Second Department of Pathology, Akita University School of Medicine, Akita 010-8543, Japan. [5]Interdisciplinary Science Center, Nihon University, Tokyo 102-0074, Japan. [6]These authors contributed equally to this work. Correspondence should be addressed to J.A. (joji@m.u-tokyo.ac.jp).

Received 3 October; accepted 3 November; published online 4 December 2005; doi:10.1038/nm1338

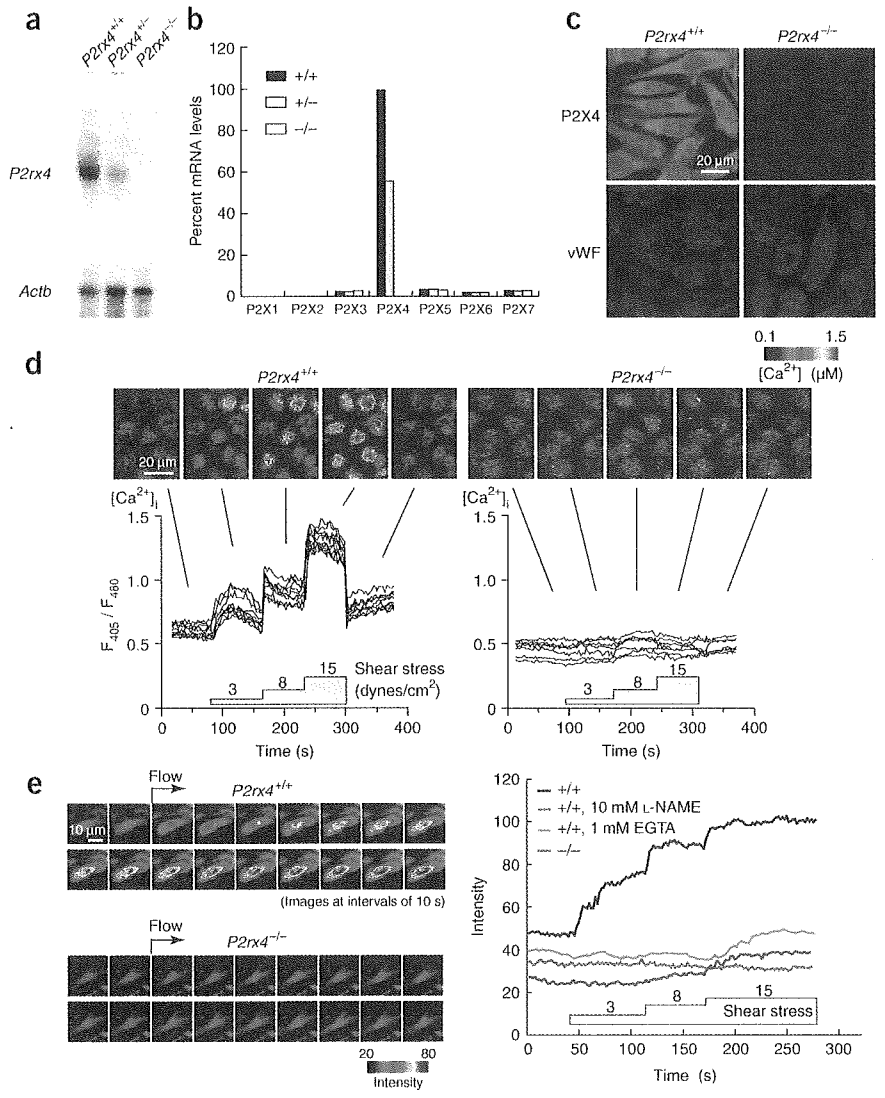

Figure 1 Impaired endothelial cell responses to flow in *P2rx4*$^{-/-}$ mice. (**a**) Northern blots of *P2rx4* mRNA from cultured pulmonary microvessel endothelial cells. The *Actb* signal was used as a loading control. (**b**) Competitive PCR analysis of the levels of mRNA encoding P2X subtypes. (**c**) Immunostaining for P2X4 receptor and an endothelial cell–specific marker, von Willebrand factor (vWF). (**d**) Flow-induced Ca^{2+} responses. Each graph represents eight $[Ca^{2+}]_i$ responses of 8–10 single cells. (**e**) Flow-induced production of NO. Left, pseudocolor images of DAF-2. Right, changes in DAF-2 intensity of 15–20 cells. Production of NO by endothelial cells of wild-type mice increased in a shear stress–dependent manner, and the increase was abolished by the NO synthase inhibitor L-NAME (10 mM) and the Ca^{2+} chelator EGTA (1 mM). Endothelial cells of *P2rx4*$^{-/-}$ mice did not show flow-induced production of NO.

wild-type mice, but no immunoreactivity in endothelial cells of *P2rx4*$^{-/-}$ mice (**Fig. 1c**). Endothelial cells of both wild-type and *P2rx4*$^{-/-}$ mice were positive for von Willebrand factor, a marker protein for endothelial cells.

The absence of P2X4 receptors impaired the response of endothelial cells to flow stimulation. When endothelial cells of wild-type mice were exposed to flow, the intracellular concentration of Ca^{2+} ($[Ca^{2+}]_i$) increased stepwise in tandem with the increases in shear stress (**Fig. 1d**), whereas no flow-induced Ca^{2+} responses occurred in endothelial cells of *P2rx4*$^{-/-}$ mice. As increases in $[Ca^{2+}]_i$ directly lead to the production of a potent vasodilator, nitric oxide (NO)[16], we examined the endothelial cells for changes in NO production with a fluorescence indicator, diaminofluorescein (DAF-2)[17]. Production of NO by endothelial cells of wild-type mice increased in response to flow, and this response was dependent on shear stress (**Fig. 1e**). Endothelial cells of *P2rx4*$^{-/-}$ mice, however, did not show flow-induced production of NO, indicating that P2X4 channels are involved in endothelial production of NO. The impaired flow-induced influx of Ca^{2+} and production of NO were rescued by *P2rx4* gene transfer using adenovirus vectors (**Fig. 2**). Adenovirus vector–mediated gene transfection was highly efficient and effective for the reintroduction of P2X4 into cultured endothelial cells. The spontaneous release of NO in healthy arteries is well known, but the exact trigger of the release remains unclear. As endothelial cells release ATP in response to shear stress, the released ATP may activate endothelial P2X4 receptors, leading to release of NO.

Increases in blood flow and administration of ATP cause vasodilation *in vivo*, and both flow- and ATP-mediated vasodilation are dependent on an intact endothelium and are mainly mediated by NO and prostaglandins[18]. We therefore examined the effects of P2X4 deficiency on the endothelium-dependent vasodilator response in mouse cremaster muscle. When acetylcholine (ACh) or ATP was administered through the jugular vein, arterioles that had been preconstricted with phenylephrine dilated in a dose-dependent manner in wild-type mice (**Fig. 3a**). In *P2rx4*$^{-/-}$ mice, however, ATP-induced vasodilation was markedly suppressed, but ACh-induced vasodilation was not suppressed at all. Occlusion of one of the branches of an arteriole with a glass micropipette increased blood flow through the other branch, and the increase in blood flow caused marked vasodilation in wild-type mice, but much less prominent vasodilation in *P2rx4*$^{-/-}$ mice (**Fig. 3b**). The blockade of NO synthesis by N^G-nitro-L-arginine methyl ester (L-NAME) markedly reduced flow-induced dilation in both types of mice. Flow-mediated vasodilator responses were also examined *ex vivo* in isolated arteries. Mesenteric arteries isolated from wild-type mice dilated in response to flow (shear stress, 20 dynes/cm^2), ATP and ACh, whereas the mesenteric arteries of *P2rx4*$^{-/-}$ mice dilated in response to ACh, but not to flow or ATP (**Fig. 3c**). The addition of EGTA or L-NAME considerably decreased flow-induced vasodilation in both types of mice, indicating that Ca^{2+} influx and NO mediate the vasodilation. The impaired flow-induced vasodilation in the *P2rx4*$^{-/-}$ mice was not the result of enhanced myogenic responses or changes in the composition or rigidity of vessel walls (**Supplementary Fig. 2** online).

No differences in external appearance, weight gain, food or water intake, or urine volume were seen between wild-type and *P2rx4*$^{-/-}$ mice during the 6-month period of the study. But we did observe a marked difference in blood pressure, as determined by intra-arterial

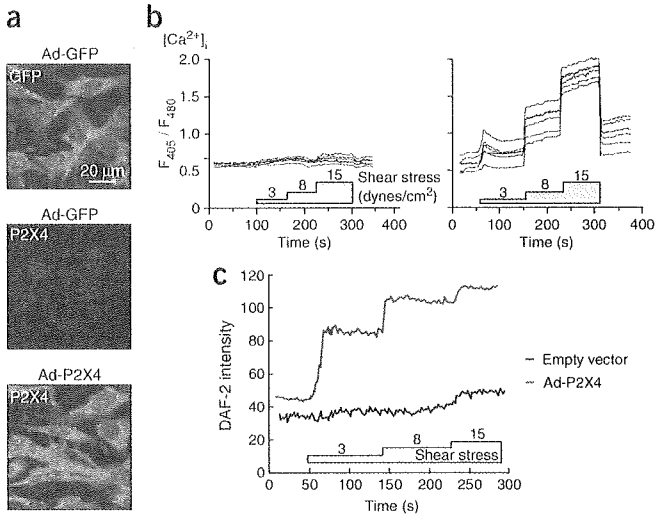

Figure 2 *P2rx4* gene transfer rescued the impaired flow-induced influx of Ca^{2+} and production of NO in cultured endothelial cells from *P2rx4*$^{-/-}$ mice. (**a**) Fluorescence photomicrographs of endothelial cells 5 d after gene transfection. Top, green fluorescent protein (GFP) expression. Ad-GFP, adenovirus vectors containing the GFP coding sequence. Center and bottom, immunostaining for the P2X4 receptor. Ad-P2X4, adenovirus vector containing mouse *P2rx4* cDNA. (**b**) Flow-induced Ca^{2+} responses. Endothelial cells transfected with Ad-P2X4 showed a shear stress–dependent increase in $[Ca^{2+}]_i$ (right), whereas endothelial cells transfected with empty vector did not (left). (**c**) Flow-induced production of NO. Production of NO by endothelial cells transfected with Ad-P2X4 increased in a shear stress–dependent manner, whereas production in endothelial cells transfected with empty vector did not. Results are representative of three experiments.

catheter measurements, with significantly higher values recorded in *P2rx4*$^{-/-}$ mice than in wild-type mice (**Fig. 4a,b**). No difference in heart rate was seen between the two groups of mice (**Fig. 4c**). But we did observe a difference in NO production. The daily amount of nitrite and nitrate (NOx) excreted in the urine was significantly less in *P2rx4*$^{-/-}$ mice than in wild-type mice (**Fig. 4d**). The decrease in NO production may be partly responsible for the increase in blood pressure in the *P2rx4*$^{-/-}$ mice.

Chronic changes in blood flow through large arteries induce structural remodeling of the vascular wall. Increases in blood flow cause enlargement of vessel diameter, whereas decreases in blood flow have the opposite effect[1,4,19]. To examine the role of the P2X4 receptor in flow-dependent vascular remodeling, we ligated the left external carotid artery of mice for 2 weeks. The ligation reduced flow in the left common carotid artery (**Supplementary Figs. 2** and **3** online), and we histologically compared the diameters of the left and the right common carotid arteries at the end of the 2-week period. Ligation of the left external carotid artery resulted in a substantial reduction in lumen diameter in the left common carotid artery in wild-type mice, but not in *P2rx4*$^{-/-}$ mice (**Fig. 4e**). The diameter of the right common carotid artery of *P2rx4*$^{-/-}$ mice was smaller than the diameter of the right common carotid artery of wild-type mice, and its walls were thicker (**Fig. 4f**), indicating that deficiency of P2X4 caused structural vascular changes under baseline conditions. The absence of flow-induced changes in diameter and the increase in medial wall thickness seen in *P2rx4*$^{-/-}$ mice resembled the structural changes that occur in eNOS-deficient mice[20], suggesting that *P2rx4* has a crucial role through endothelial production of NO in controlling vascular structural adaptation to chronic changes in blood flow.

A considerable amount of research has been devoted to the mechanotransduction of shear stress in endothelial cells. But the identity of shear stress receptors and the final signaling pathways they evoke remain unclear. Several endothelial proteins and structures,

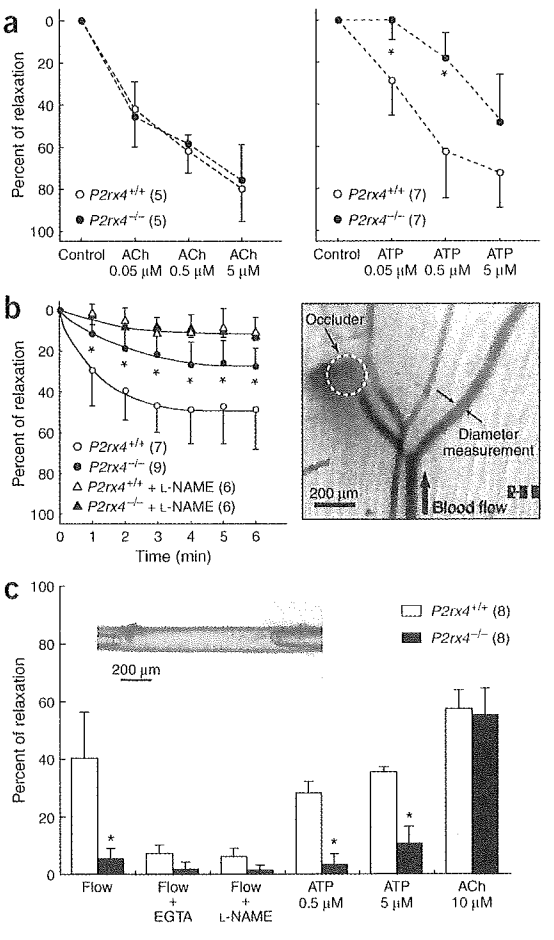

Figure 3 Impaired vasodilatory responses in *P2rx4*$^{-/-}$ mice. We examined cremaster muscle arterioles and mesenteric arteries for changes in diameter in response to various stimuli. Changes in vessel diameter are expressed as percentages: 0% represents the diameter of the vessel constricted with phenylephrine (10 μM), and 100% represents the diameter of the vessel dilated with papaverine (5 mM). (**a**) Vasodilatory response of cremaster muscle arterioles to ACh and ATP. Injection of ACh or ATP through the jugular vein induced marked vasodilation in both wild-type and *P2rx4*$^{-/-}$ mice, but vasodilation induced by ATP was significantly less in *P2rx4*$^{-/-}$ mice. (**b**) Vasodilatory response of cremaster muscle arterioles to flow. One of the branches of an arteriole was compressed with a glass micropipette (Occluder) to stop blood flow, and the other branch, in which the blood flow increased, was examined for changes in diameter. Dilation in response to increased blood flow occurred in wild-type mice, but the response was much weaker in *P2rx4*$^{-/-}$ mice. Administration of L-NAME significantly reduced the flow-induced dilation in both types of mice. (**c**) Vasodilatory response of mesenteric arteries. Data are reported as percentage relaxation 5 min after application of each stimulus, when maximum response was observed. Flow- or ATP-induced dilation was significantly weaker in *P2rx4*$^{-/-}$ mice compared with wild-type mice. Addition of EGTA or L-NAME markedly suppressed flow-induced vasodilation in both types of mice. Sample numbers are indicated in parentheses. $^*P < 0.01$.